

See discussions, stats, and author profiles for this publication at: <https://www.researchgate.net/publication/263939784>

Hierarchical Structure–Property Relationships in Graft-Type Fluorinated Polymer Electrolyte Membranes Using Small- and Ultrasmall-Angle X-ray Scattering Analysis

ARTICLE *in* MACROMOLECULES · MARCH 2014

Impact Factor: 5.8 · DOI: 10.1021/ma500111x

CITATIONS

4

READS

31

8 AUTHORS, INCLUDING:



Masato Ohnuma

National Institute for Materials Science

29 PUBLICATIONS 160 CITATIONS

[SEE PROFILE](#)



Yosuke Katsumura

The University of Tokyo

268 PUBLICATIONS 2,800 CITATIONS

[SEE PROFILE](#)

Hierarchical Structure–Property Relationships in Graft-Type Fluorinated Polymer Electrolyte Membranes Using Small- and Ultrasmall-Angle X-ray Scattering Analysis

Tran Duy Tap,^{†,‡} Shin-ichi Sawada,[†] Shin Hasegawa,[†] Kimio Yoshimura,[†] Yojiro Oba,[§] Masato Ohnuma,[§] Yosuke Katsumura,[‡] and Yasunari Maekawa^{*,†}

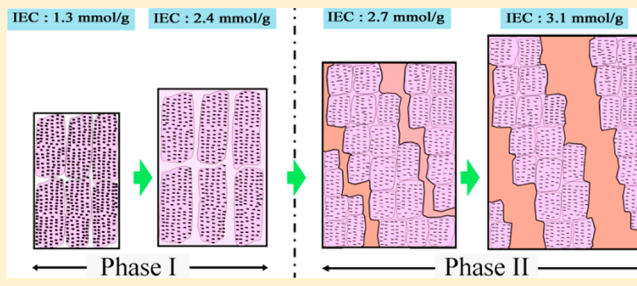
[†]High Performance Polymer Group, Quantum Beam Science Directorate, Japan Atomic Energy Agency (JAEA), 1233 Watanuki, Takasaki, Gunma 370-1292, Japan

[‡]Department of Nuclear Engineering and Management, Graduate School of Engineering, The University of Tokyo, 7-3-1 Hongo, Bunkyo-ku, Tokyo 113-8656, Japan

[§]Quantum Beam Center, National Institute for Materials Science (NIMS), 1-2-1 Sengen, Tsukuba, Ibaraki 305-0047, Japan

S Supporting Information

ABSTRACT: The hierarchical structures of graft-type poly(ethylene-*co*-tetrafluoroethylene) (ETFE)-based polymer electrolyte membranes (ETFE-PEMs) were investigated using small- and ultrasmall-angle X-ray scattering experiments. The ETFE-PEMs with ion exchange capacities (IECs) < 2.4 mmol/g possessed conducting graft domains around lamellar crystals, with a *d*-spacing of 21.8–29.1 nm, and oriented crystallites (lamellar grains) with short and long correlation distances of 218–320 and 903–1124 nm, respectively. The membranes with IECs > 2.7 mmol/g showed a new phase of crystallite network domains with a *d*-range of 225–256 nm, indicating a phase transition from oriented crystallite to crystallite network structures in the IEC range of 2.4–2.7 mmol/g. Noted that for the ETFE-PEMs with high IECs higher conductivity at 30% RH and compatible tensile strengths at 100% RH and 80 °C, compared with Nafion, originated from the well-interconnected ion channels around the crystallites and the remaining lamellar crystals and crystallites, respectively.



1. INTRODUCTION

Polymer electrolyte membranes (PEMs) are key materials for polymer electrolyte fuel cells, which have attracted much interest for solving environmental problems because their clean and efficient power generation is expected to reduce fossil fuel consumption. For high fuel cell performance, PEMs must possess certain characteristics including high proton conductivity, high chemical and thermal stability, low fuel permeability, moderate water uptake, and good mechanical strength.¹ Up to now, perfluorosulfonic acid (PFSA) membranes such as Nafion have been widely used as PEM materials because of their excellent chemical and physical stability and high proton conductivity. However, PFSA membranes suffer critical drawbacks, such as high fuel crossover, limited operation temperature (<80 °C) in fuel cells, and high cost. Under some of the more severe operating conditions requested by industry (>80 °C, <50% RH), the proton conductivity of PFSA membranes drops significantly, leading to a decrease in fuel cell performance.^{2–4} Thus, it is crucial to develop new PEM materials that exhibit high levels of proton conductivity at high temperatures under low relative humidity (RH) as well as superior mechanical properties under humidified conditions.

Preirradiation grafting, in which polymer substrates are first irradiated using a quantum beam and then immersed in a monomer solution for graft polymerization, is a widely recognized technique for the introduction of a new functional graft polymer phase directly into polymer substrates while maintaining the inherent characteristics of the substrates such as thermal stability, mechanical strength, and crystallinity.⁵ Therefore, this radiation technique has been applied to the preparation of graft-type PEMs for fuel cells using graft monomers possessing an ion-conducting group (i.e., sulfonic acid) grafted onto fluorinated polymer films and fully aromatic hydrocarbon polymers such as poly(ether ether ketone).^{6,7} Among the fluorinated graft-type PEMs, poly(styrenesulfonic acid)-grafted poly(ethylene-*co*-tetrafluoroethylene) (ETFE) (ETFE-PEM) has been intensively investigated in our group^{8–12} and others^{13–16} as a promising graft-type PEM material because of its well-balanced properties, which are required for graft polymerization as well as fuel cell application, such as high proton conductivity, mechanical strength, and thermal/chemical stability.

Received: January 15, 2014

Revised: March 14, 2014

Published: March 21, 2014

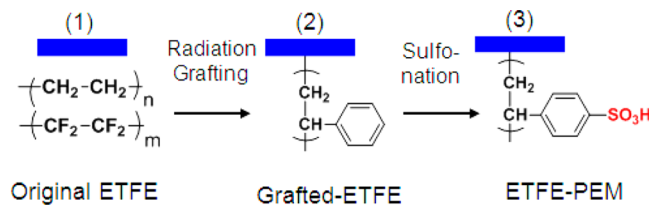
Proton conductivities of PEMs drop significantly under low RH, leading to the decreases of power generation in fuel cells; at the same time, mechanical properties under a humidified condition (100% RH) are an important parameter for durability under severe operating conditions, such as flooding in fuel cell systems because the absorption of large amounts of water induces stress in PEMs, resulting in the degradation. Recently, we reported the relative humidity (RH) dependence of the electrochemical and mechanical properties of ETFE-PEMs in a wide ion exchange capacity (IEC) range at 80 °C.¹⁷ Unlike aromatic hydrocarbon-type PEMs, ETFE-PEMs have proton conductivities that are less dependent on the RH. As a result, ETFE-PEMs with IECs > 2.7 mmol/g exhibited higher conductivity (>0.009 S/cm) under 30% RH and showed compatible tensile strengths of approximately 10 MPa at 100% RH and 80 °C.¹⁷

Fundamental understanding of the structure–property relationships of PEMs is crucial for the improvement of their performance, durability, and cost. Therefore, it is important to analyze the hierarchical structures of PEMs, such as the crystalline morphology, conducting layers (ion channels) consisting of graft polymers, internal structures of the conducting layers such as aggregation of ionic groups and water, and the hydrophobic/hydrophilic phase separation structures.^{6,18–21} The previous structural analyses of ETFE-based PEMs using SAXS and SANS covered a *q*-range higher than 0.1 nm⁻¹, resulting in discussions mainly for lamellar structures.^{22,23} As a graft-type PEM, poly(styrenesulfonic acid) with cross-linked polytetrafluoroethylene (cPTFE-PEM) was investigated over a wide *q*-range (*q* = 4 × 10⁻³–1.5 nm⁻¹) by the combination of small-angle X-ray/neutron scattering (SAXS/SANS), while the hierarchical structure analysis of the cPTFE-PEMs was limited for those with GDs lower than 36%.²⁴ However, to our knowledge, there has been no comprehensive analysis of the hierarchical structures of grafted membranes with a wide range of graft polymer contents (up to 100%) and sizes (1 nm to 1 μm) for elucidating the structure–property relationships of PEMs. Thus, the hierarchical structures of ETFE-PEMs over an IEC range of 0–3.1 mmol/g (GDs = 0–117%) were observed using a wide *q*-range observation (*q* = 4 × 10⁻³–3 nm⁻¹) in small- and ultrasmall-angle X-ray scattering (SAXS/USAXS), corresponding to a large Bragg spacing (*d*-spacing) of 2–1600 nm. The results were compared with the profiles of the precursor original ETFE and polystyrene-grafted ETFE films because grafted PEMs are well-known to retain the crystalline structures and graft polymer phases of the precursor original and grafted films. The hierarchical structures of the ETFE-PEMs as characterized by SAXS measurements were supported by field emission scanning electron microscopy (FE-SEM) observations. On the basis of the results obtained from the SAXS measurements and the SEM observations, the relationship of the hierarchical structures to the electrolyte properties such as proton conductivity, water uptake, crystallinity, and mechanical strength is discussed.

2. EXPERIMENTAL SECTION

2.1. Sample Preparation and Characterization. ETFE-PEMs with GDs of 4.2–117% were prepared by preirradiation grafting of styrene and a subsequent sulfonation reaction, as showed in Scheme 1. Because the detailed preparation method was described in our previous publications,¹⁷ the present study briefly outlines the preparation method as follows. ETFE films with a thickness of 50

Scheme 1. Radiation-Induced Graft Polymerization of Styrene (2) onto an ETFE Substrate (1) and the Subsequent Sulfonation To Prepare ETFE-PEM (3)



μm (Asahi Glass Co. Ltd.) were preirradiated by ⁶⁰Co γ -rays with an absorbed dose of 15 kGy under an argon atmosphere and then immersed in a styrene solution at 60 °C. The GD of the grafted-ETFE was determined using the equation

$$\text{GD (\%)} = \frac{W_g - W_0}{W_0} \times 100\% \quad (1)$$

where W_0 and W_g are the weights of the films before and after the graft polymerization, respectively. The grafted-ETFE was then immersed in 0.2 M chlorosulfonic acid in 1,2-dichloroethane at 50 °C for 6 h. The membrane was washed with pure water at 50 °C for 24 h to obtain an ETFE-PEM. The IECs of the ETFE-PEMs were determined by titration analysis with a standardized 0.01 M NaOH solution using the equation

$$\text{IEC (mmol/g)} = \frac{0.01 \times V_{\text{NaOH}}}{\text{dry weight of membrane}} \quad (2)$$

where V_{NaOH} is the consumed volume (mL) of the 0.01 M NaOH solution.

The proton conductivities under 30% RH and the mechanical strength under 100% RH were measured at 80 °C using our standard procedures described in the previous paper.¹⁷

2.2. SAXS Measurements. SAXS measurements were performed using two in-house SAXS spectrometers (NIMS-SAXS-II and NIMS-SAXS-III) at the National Institute of Material Science (NIMS) and at USAXS at Super Photon ring-8 GeV (SPring-8), Japan. At NIMS, fine-focus SAXS instruments with X-rays of Mo K_α ($\lambda_{\alpha} = 0.07$ nm) (Rigaku NANO-Viewer, Tokyo, Japan) and Cr K_α ($\lambda_{\alpha} = 0.23$ nm) (Bruker NanoSTAR, Germany) were utilized. The characteristic K_α radiation was selected and focused by two-dimensional confocal mirrors and Göbel mirrors for Mo- and Cr-SAXS, respectively. The 2D scattering X-rays were then recorded using a multiwire gas-filled 2D detector (Bruker, HiStar, Germany). The sample–detector distances in the Mo-SAXS and Cr-SAXS were 35.0 and 105.6 cm, respectively. Therefore, the total *q*-range of the SAXS profiles at NIMS was *q* = 0.07–3.13 nm⁻¹. Here, *q* is referred to as the modulus of the scattering vector, equaling $4\pi \sin \theta / \lambda$, where 2θ is the scattering angle and λ is the wavelength of the incident X-rays. At SPring-8, SAXS measurements were performed by USAXS at beamline BL19B2 using an incident X-ray energy of 18 keV ($\lambda = 0.0688$ nm). The scattering X-rays were detected by the two-dimensional hybrid pixel array detectors, PILATUS-2 M (pixel apparatus). The sample–detector distance was 42 m, corresponding to a *q*-range of 0.004–0.242 nm⁻¹. Thus, both pinhole SAXS measurements at NIMS and SPring-8 were carried out to cover a wide *q*-range (*q* = 0.004–3.13 nm⁻¹). The SAXS intensities were circularly averaged and corrected for the absorption of the sample and the instrument background. The absolute SAXS intensity was corrected using the secondary standard of glassy carbon (provided by Argonne National Laboratory).²⁵ Hydrated samples had been measured twice consecutively (at an interval of ca. 3 min) at SPring-8 to obtain SAXS profiles to ensure that there were no artifacts due to the evaporation of water. Figure S1 (Supporting Information) shows the SAXS profiles of the ETFE-PEM with a GD of 117%, which possessed the highest water uptake (145%). The identical SAXS profiles of the two measurements indicate that no variation in the SAXS data was detected. At NIMS, the samples equilibrated in pure

water were placed in cells with Kapton windows to prevent evaporation.

2.3. FE-SEM Observation. The surface and cross-sectional images of the pristine ETEF, grafted-ETFE, and ETEF-PEMs were observed by a JEOL JSM-6700F field emission-scanning electron microscope (FE-SEM). The membranes were stained with silver by ion exchange of the sulfonic acid groups by immersing it in a large excess of 0.5 M AgNO₃ solution for 14 h, followed by rinsing with deionized water for 1 day at RT and drying in a vacuum oven at 40 °C for 12 h. For cross-sectional imaging, the samples were embedded in an epoxy resin and sectioned using a microtome. All the membranes were sputtered with a 10 nm gold layer. Images were obtained using a secondary electron imaging mode of FE-SEM with an accelerating voltage of 5 kV.

3. RESULTS AND DISCUSSION

3.1. Variation of the Hierarchical Structure by Preparation Procedure. Since the grafted PEMs are well-known to maintain to some extent the crystalline structures of precursor original ETEF and polystyrene grafted films (grafted-ETFE), one of the advantages for graft-type PEMs is to characterize more precisely by comparing with those of the precursor films. Thus, the morphology changes in the higher-order structures according to the preparation procedures of the pristine ETEF and grafted-ETFE with a GD of 59% were compared with ETEF-PEM with an IEC of 2.4 mmol/g.

Figure 1a shows the overall SAXS profiles of the original ETEF, grafted-ETFE with a GD of 59% and ETEF-PEM

(slopes, shoulders, and peaks) of the original ETEF, grafted-ETFE, and ETEF-PEM, the scattering profiles were classified into two q regions: q -region I ($q = 1.5 \times 10^{-1}$ – 3 nm^{-1} , $d = 2$ – 40 nm) and q -region II ($q = 4 \times 10^{-3}$ – $1.5 \times 10^{-1} \text{ nm}^{-1}$, $d = 40$ – 1600 nm).

Over the entire q -range, the SAXS profile of the pristine ETEF film possessed only a pronounced peak at approximately $q = 0.272 \text{ nm}^{-1}$ with a d -spacing of 23.1 nm, originating from a lamellar structure, as previously reported.^{18,19} Figure 1b showed the Lorentz-corrected SAXS profiles of the pristine ETEF, grafted-ETFE, and ETEF-PEM.^{26,27} The Lorentz-corrected SAXS profiles of the original ETEF film showed the peak at $q = 0.366 \text{ nm}^{-1}$, corresponding to a lamellar spacing of 18.8 nm.

For the grafted-ETFE, in q -region I, a shoulder-like peak at $q_1 = 0.192 \text{ nm}^{-1}$ ($d_1 = 28.7 \text{ nm}$) appeared at a similar q -position as in the pristine ETEF film, indicating the generation of a new phase consisting of polystyrene (PS)-grafted polymers (grafts) under the influence of the lamellar structure of the pristine ETEF film. In other words, this shoulder-like peak originated from the correlation distance of the primary lamellar stacks. It should be noted that the d -spacing of the grafted-ETFE is 9.9 nm larger than that of the pristine ETEF film. This expansion indicates that some of the PS grafts were introduced in the lamellar amorphous regions (Figure 2). Furthermore, the scattering intensity $I(q_1)$ of the grafted-ETFE film is higher than that of the pristine ETEF film, indicating that the PS grafts, which have a lower electron density, were introduced in the lamellar amorphous domains, resulting in an increase in the scattering contrast between the ETEF lamellar crystalline domains (higher electron density) and the amorphous domains consisting of the ETEF lamellar amorphous region and PS grafts (lower electron density).

In q -region II, a shoulder-like peak at approximately $q_2 = 0.0236 \text{ nm}^{-1}$ ($d_2 = 266 \text{ nm}$) was observed, while there was no appreciable scattering in the pristine ETEF film. The shoulder-like peak (q_2) is expected to originate from the crystallites (lamellar grains) including the PS grafts in the amorphous phases. In addition, the SAXS profiles of the grafted-ETFE exhibited another shoulder-like peak in q -region II at $q_3 = 0.0060 \text{ nm}^{-1}$ ($d_3 = 1050 \text{ nm}$). One possible explanation for the peaks q_2 and q_3 , should be a set of correlation distances, d_2 and d_3 , for the short and long periods, respectively, of the oriented crystallites (Figure 2).

Because the SAXS profile of the ETEF-PEM exhibited three similar shoulder-like peaks to those of the grafted-ETFE over the entire q -range, it was clear that the introduction of sulfonic acid groups via sulfonation of the PS grafts induced little change in the correlation distances of the lamellar stacks and crystallites, as shown in Figure 1. Thus, the grafted regions consisting of PSSA, which act as ion channels, are formed during the radiation-induced graft polymerization step. Contrary to the graft polymerization process, the expansion of the lamellar d -spacing (d_1) of the grafted-ETFE by the sulfonation process (i.e., the d -spacing difference between the grafted-ETFE and the ETEF-PEM) is very small (only 0.4 nm), indicating that the introduction of the sulfonic acid groups in the graft domains did not enlarge the total lamellar spacing (Figure 2).

3.2. Variation of the Hierarchical Structure with the Grafting Degree. Figures 3a and 4a show the SAXS profiles of the grafted-ETFE films with GDs of 0–117% and the corresponding ETEF-PEMs with IECs of 0–3.1 mmol/g in

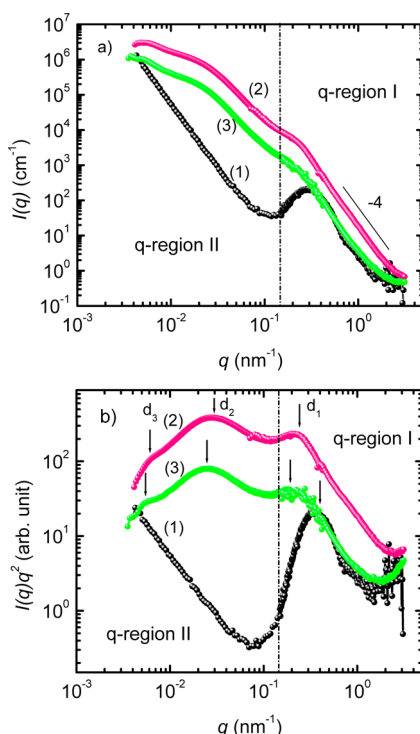


Figure 1. (a) SAXS profiles of the (1) original ETEF, (2) grafted-ETFE with a GD of 59%, and (3) ETEF-PEM with an IEC of 2.4 mmol/g. (b) Lorentz-corrected SAXS profiles of the original SAXS profiles in (a).

(sulfonated form of the grafted-ETFE) with an IEC of 2.4 mmol/g in the q -range of 4×10^{-3} – 3 nm^{-1} . The combined small-angle scattering method using USAXS and SAXS measurements enables the determination of the hierarchical structures of those membranes over a wide range in real d -spacing (2–1600 nm). According to the scattering features

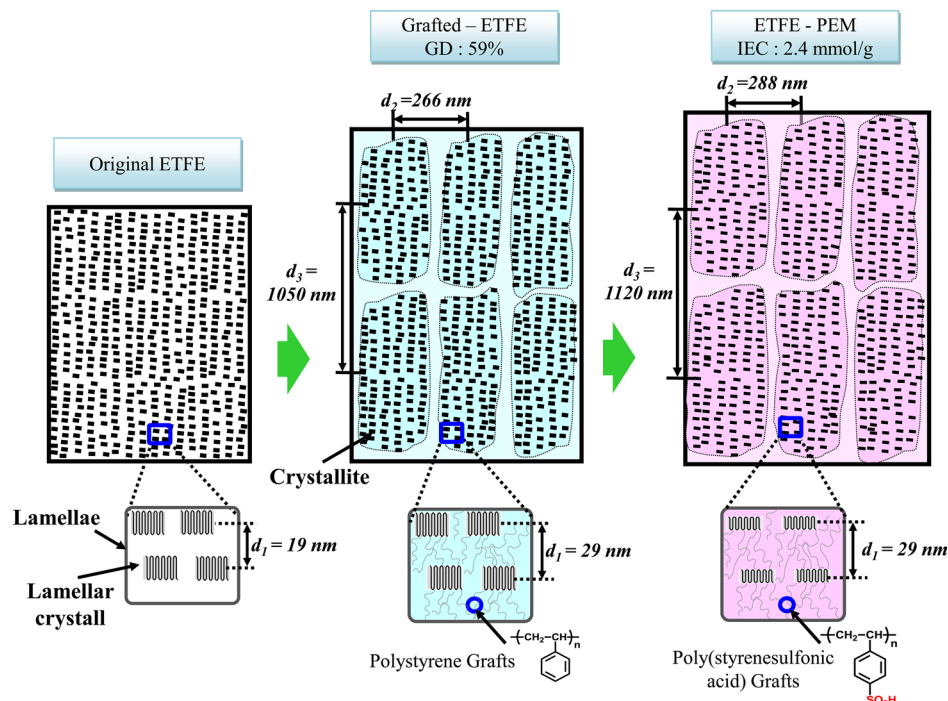


Figure 2. Schematic illustrations of the morphology change in the higher-order structures according to the preparation procedures of the pristine ETFE, grafted-ETFE with a GD of 59%, and ETFE-PEM with an IEC of 2.4 mmol/g.

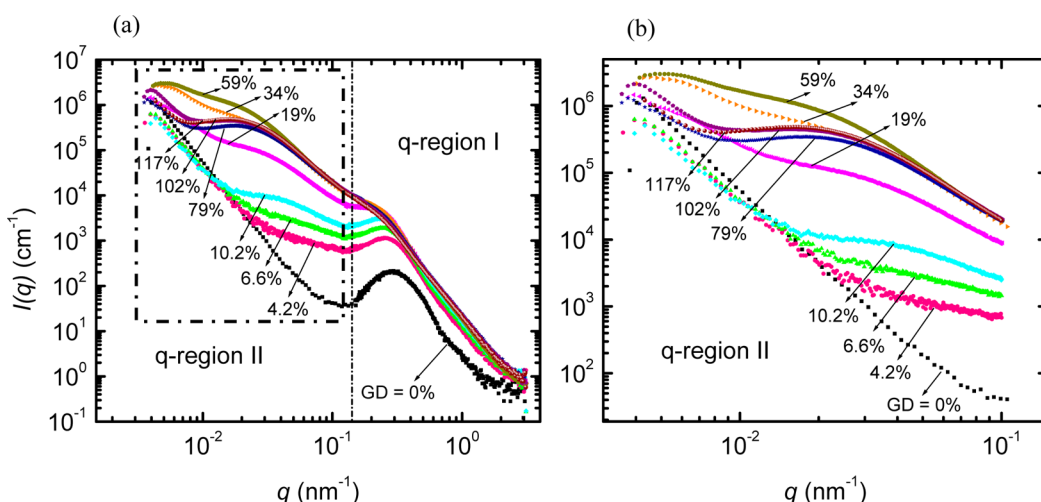


Figure 3. (a) SAXS profiles of the grafted-ETFE with GDs of 0–117%. (b) Scattering profiles in the low q -region (q -region II: $q = 4.0 \times 10^{-3} \text{ to } 1.5 \times 10^{-1} \text{ nm}^{-1}$) were enlarged.

the q -range of 4×10^{-3} – 3.0 nm^{-1} . The scattering profiles in the low q -region (q -region II: $q = 4.0 \times 10^{-3}$ – $1.5 \times 10^{-1} \text{ nm}^{-1}$) are enlarged in Figures 3b and 4b. The GD and IEC dependence of the scattering profiles of the grafted-ETFE and ETFE-PEM films are different in q -region I and q -region II.

q -Region I ($q = 1.5 \times 10^{-1}$ – 3 nm^{-1} , $d = 2$ – 40 nm). **Grafted-ETFE.** The SAXS profiles of the grafted-ETFE exhibited clear peaks in the GD range of 4.2–19%, which became broader shoulder-like peaks at higher GDs (34–117%) in q -region I. Thus, the lamellar period ($d_1 = 2\pi/q_1$) and scattering intensities at q_1 in the Lorentz-corrected SAXS profiles of the grafted-ETFE films (Supporting Information, Figure S2a) were plotted as a function of the GD (Figure 5). The lamellar period of the grafted-ETFE increased from 18.8 to 28.7 nm by increasing GDs from 0% (pristine ETFE) to 59%

and remained constant in the GD range from 59 to 117%. From the results of Figure 5a, the PS grafts were introduced only at the early stage of the radiation-induced graft polymerization ($GD < 59\%$) and were generated outside the lamellar stacks with GDs higher than 59%. Furthermore, even for the grafted-ETFE with a GD lower than 59%, the lamellar period dramatically increased at the early stage of grafting, i.e., $GD < 10.2\%$ (18.8 nm (pristine ETFE film) to 23.4 nm at $GD = 10.2\%$), while it gradually increased in the GD range of 10.2–59% (23.4 nm at $GD = 10.2\%$ to 28.7 nm at $GD = 59\%$). The SAXS intensities $I(q_1)$ of the grafted-ETFE increased dramatically with the increase of the GD from 0 to 34% and gradually decreased as the GD increased above 34% (Figure 5b). Although the introduction of PS grafts into the lamellar amorphous phases increases the scattering contrast, the $I(q_1)$ of

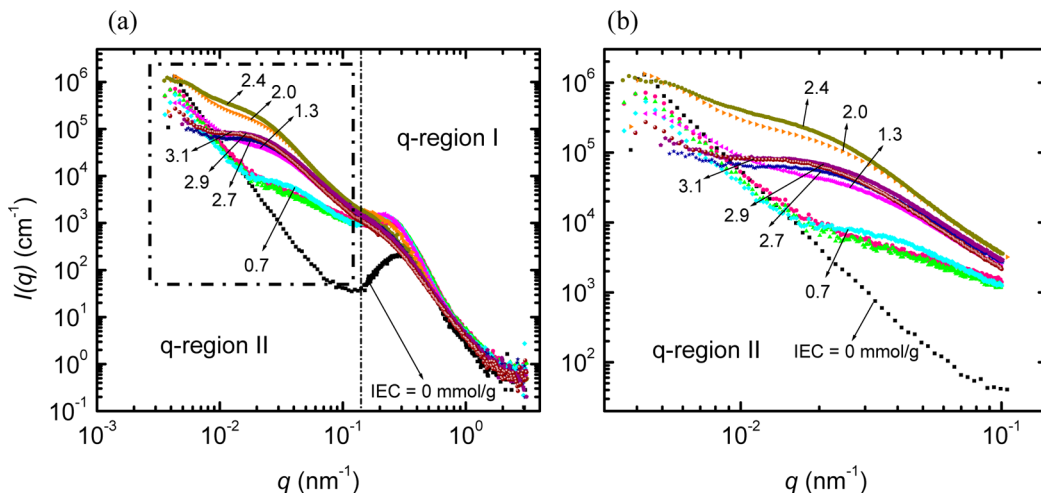


Figure 4. (a) SAXS profiles of the ETFE-PEMs with IECs of 0–3.1 mmol/g. (b) Scattering profiles in the low q -region (q -region II: $q = 4.0 \times 10^{-3}$ – 1.5×10^{-1} nm⁻¹) were enlarged.

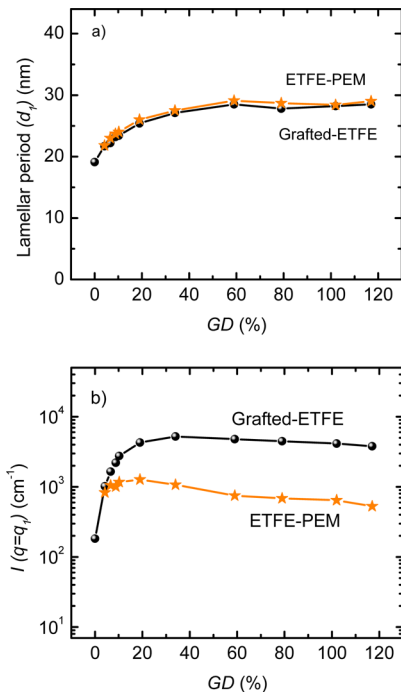


Figure 5. GD dependences of the (a) lamellar period (d_1) and (b) peak-scattered intensity at $q = q_1$ of the grafted-ETFE and ETFE-PEM.

the grafted-ETFE with GDs of 34–117% slightly decreased. This slight decrease in the intensity should correspond to the fact that the crystallinity of the pristine ETFE decreased by only 10% for the graft polymerization with a GD of 117%.¹⁷

ETFE-PEM. As shown in Figure 4, the SAXS profiles of the ETFE-PEMs were almost the same as those of the grafted-ETFE in q -region I over the entire IEC (or GD) range. The lamellar periods (d_1) and scattering intensities at q_1 in the Lorentz-corrected SAXS profiles of the ETFE-PEMs (Supporting Information, Figure S2b) are also plotted as a function of the GD in Figure 5. The increases of the lamellar periods of the ETFE-PEMs, resulting from the introduction of the sulfonic acid groups onto the grafted-ETFE, were restricted (less than 1 nm) over the entire IEC range.²⁸ The SAXS intensities of the ETFE-PEMs increased with the increases of GD over the range of 4.2–19% and then gradually decreased as GD increased

above 19%. As previously reported, the decrease in the crystallinity (deterioration of the lamellar stacks) is due to the sulfonation reaction but not the irradiation and successive graft polymerization processes.¹⁷ Taking into account the fact that no decrease of the lamellar periods was observed while the crystallinity decreased during the sulfonation, the lamellar crystals became thinner, while the lamellar stacks did not deteriorate. It should be noted that even upon introducing higher amounts of grafted polymer to the original ETFE by weight (GDs up to 117%), the lamellar stacks are maintained, although with some extent of decreasing crystallinity.

The increasing lamellar period with increasing IEC for the ETFE-PEMs was similar to the behavior observed for cPTFE-PEM. The lamellar period of cPTFE-PEM increased at a very early stage of the graft polymerization with a GD range of only up to 5% and then remained constant for GDs > 5%.²⁴ In contrast, for the ETFE-PEMs, the lamellar stacks were enlarged by the introduction of additional PSSA grafts with the increase of GDs in a larger range (GDs < 59%) (IECs < 2.4 mmol/g) (Figure 5a). These results can be explained by the assumption that partially fluorinated ETFE is less stiff than fully fluorinated PTFE, resulting in less steric restriction for the expansion of lamellar crystals by the insertion of polystyrene grafts.

q -Region II ($q = 4 \times 10^{-3}$ – 1.5×10^{-1} nm⁻¹, $d = 40$ – 1600 nm). **Grafted-ETFE.** The grafted-ETFE with GDs ranging from 19 to 59% showed two shoulder-like peaks in q -region II, which were related to a set of correlation distances of the oriented crystallites consisting of lamellar grains, as mentioned in section 3.1. Thus, two correlation distances for the crystallites, d_2 and d_3 , were estimated from the Lorentz-corrected SAXS profiles (Supporting Information, Figure S2a). The d_2 values and the scattering intensities at $q = q_2$ are plotted as a function of the GD (Figure 6). The d_2 values of the grafted-ETFE increased from 141 to 266 nm with increasing GD from 10.2 to 59%. Three grafted-ETFE films with GDs of 19, 34, and 59% showed clear extra peaks at $q_3 = 6.59 \times 10^{-3}$, 6.12×10^{-3} , and 5.96×10^{-3} nm⁻¹, corresponding to $d_3 = 952$, 1030, and 1050 nm, respectively. Increases in d_2 and d_3 with the increasing GD in the range of 19–59% were observed, strongly indicating a volume increase of the amorphous domains resulting from the introduction of PS grafts between the crystallites together with the lamellar amorphous region, as confirmed by the increase in d_1 (Figure 5a).

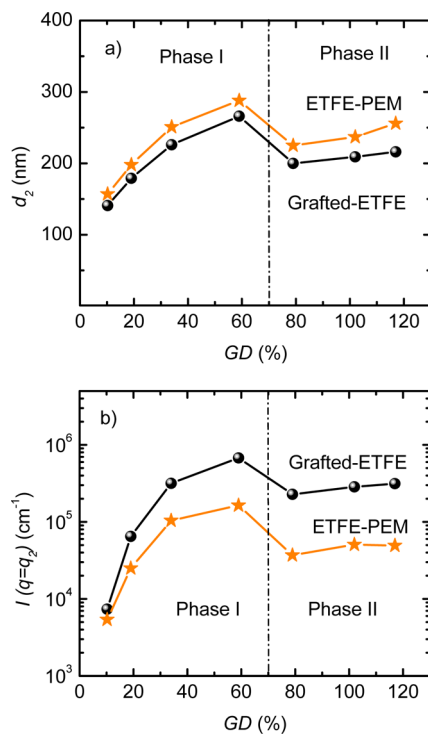


Figure 6. GD dependences of the (a) d_2 -spacing and (b) peak-scattered intensity at $q = q_2$ of the grafted-ETFE and ETFE-PEM.

The scattering contrast between the inside and outside of the crystallites increased with the increase of the GD and became high for the grafted-ETFE films with GDs higher than 10.2% because the introduction of the PS grafts lowers the electron density, resulting in an enhancement of the contrast between the inside and outside of the crystallites. Accordingly, oriented crystallites in q -region II (d_2 and d_3) were observed in the grafted-ETFE with GDs from 19 to 59% but not for that with a GD lower than 10.2%.

The scattering profiles for GDs of 79–117%, which were totally different from those for GDs of 19–59%, showed only shoulder-like peaks at $q_2 = 2.91 \times 10^{-2}$ – $3.14 \times 10^{-2} \text{ nm}^{-1}$ ($d_2 = 200$ – 216 nm). The d_2 of the grafted-ETFE suddenly decreased from 266 to 200 nm with an increase in the GD from 59 to 79% and then slightly increased from 200 to 216 nm with an increase in the GD from 79 to 117%. It should be noted that $I(q_2)$ of the grafted-ETFE with a GD of 79% decreased to only 34% of that of the membrane with a GD of 59%. The discontinuous changes in d_2 and $I(q_2)$ of the grafted-ETFE in the GD range of 59–79% strongly indicate a phase transition of the grafted-ETFE morphology induced by the introduction of the PS grafts; thus, in this paper, we define the two phases of the grafted-ETFE with GDs in the range of 0–59% and 79–117% as phase I and phase II, respectively.

Contrary to the discontinuous change in d_2 and $I(q_2)$ from phase I to II with GDs of 59–79%, the SAXS profiles in phase I, i.e., d_1 and $I(q_1)$, are constant. This scattering behavior clearly shows that the amorphous PS grafts were excluded at the intercrystallite regions but not at interlamellar regions, resulting in the formation of a new amorphous domain consisting of only PS grafts outside of the crystallites. This kind of morphological change has been reported in crystalline/amorphous polymer blends such as crystalline poly(vinylidene fluoride) (PVDF)/amorphous poly(methyl methacrylate) (PMMA) and crystallite polycaprolactone (PCL)/amorphous polycarbonate (PC).^{29,30} In the reports cited above, at lower contents, the amorphous polymers are completely miscible with the crystalline polymers in the lamellar amorphous regions, whereas at higher contents, the amorphous polymers were excluded from the interlamellar and/or intercrystallite regions and new amorphous polymer regions were formed. Even though phase II possesses new amorphous PS graft regions, the lamellar and crystallite structures (d_1 and d_2) were maintained. Furthermore, upon increasing the GD above 79%, d_1 , d_2 , $I(q_1)$, and $I(q_2)$ were almost constant, even though the contents of the amorphous PS grafts increased 1.5 times in weight. These observations led us to a new structural model for phase II, in which there are

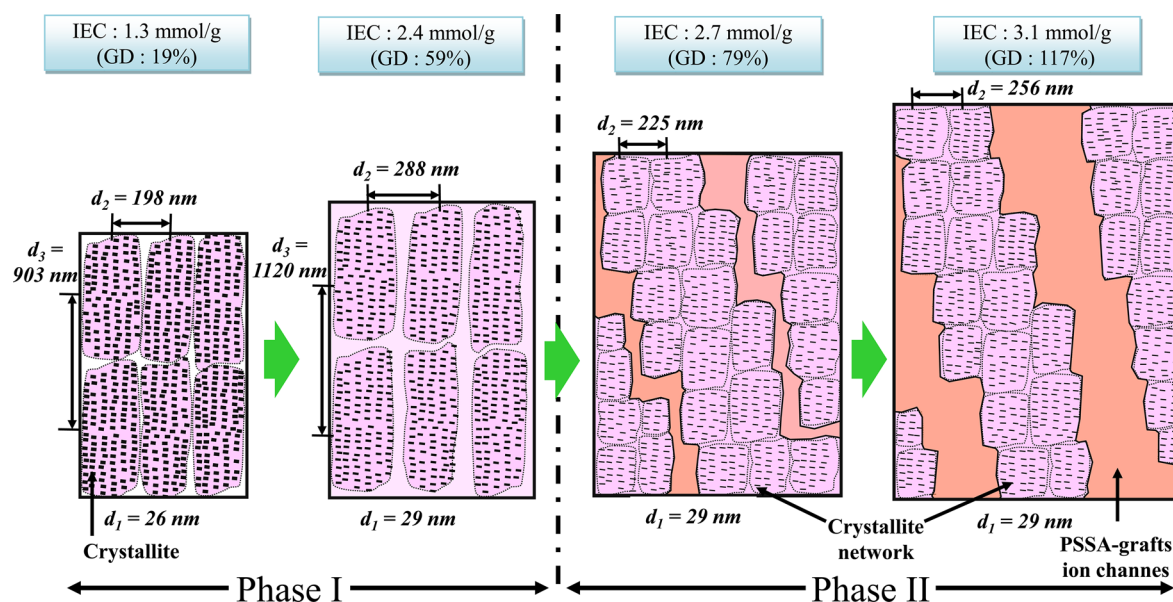


Figure 7. Schematic illustrations of the morphology change in the higher-order structures of the ETFE-PEMs as a function of the IEC: IEC = 1.3–3.1 mmol/g. The schematic picture of the PEM with IEC = 2.4 mmol/g is corresponding to the ETFE-PEM shown in Figure 2.

two large scale domains: “an amorphous PS graft domain” and “a crystallite network domain”, consisting of well-connected crystallites (lamellar grains) with correlation distances (d_2) of 200–216 nm. Accordingly, as a function of the GD, the hierarchical structures of the grafted-ETFE films change with the phase transition from phase I to II, as illustrated in Figure 7, which refers to the phase separation of the crystalline/amorphous polymer blends.^{29,30}

ETFE-PEM. All the ETFE-PEMs with different IECs exhibited similar scattering profiles to those of the corresponding precursor grafted-ETFE films in q -region II (Figure 4). Thus, the sulfonation process did not affect the structures of the grafted-ETFE with any GD on a scale larger than 40 nm, as was observed in q -region I. The correlation distances d_2 and the scattering intensities $I(q_2)$ in the Lorentz-corrected SAXS profiles of the ETFE-PEMs (Supporting Information, Figure S2b) are plotted as a function of the GD in Figure 6. In addition, extra peaks for IECs of 1.3, 2.0, and 2.4 mmol/g were observed at $q_3 = 6.96 \times 10^{-3}$, 6.02×10^{-3} , and 5.59×10^{-3} nm⁻¹, corresponding to $d_3 = 903$, 1044, and 1124 nm in q -region II, and these peaks increased as the IEC increased, as observed in the grafted-ETFE.

In the entire IEC range, the correlation distances of the crystallites d_2 of the ETFE-PEMs are higher than those of the grafted-ETFE films by 8–18%, in contrast to the slight change in the lamellar stacks (d_1) (Figures 5a and 6a). Note that the discontinuous changes in q_2 and $I(q_2)$ of the ETFE-PEMs were observed in the IEC region between 2.4 and 2.7 mmol/g, which apparently corresponds to the GD region (59–79%) for the phase transition in the precursor grafted-ETFE. Thus, it is very clear that the morphology of the ETFE-PEMs, phase I or phase II, can be determined by the phase transition resulting from the introduction of the PS grafts during the grafting process but not the sulfonation process. As a result, the ion channels are composed of PSSA grafts localized around the lamellar crystals in phase I. For IECs > 2.4 mmol/g, the ETFE-PEMs have an extra phase consisting of only PSSA grafts together with the two phases existing in phase I. Similar crystallite structures were observed in cPTFE-PEM in the low q -range of 5×10^{-3} – 3×10^{-2} nm⁻² by SANS measurements, and the intensity of the corresponding peaks increased dramatically with increasing GD from 6.2 to 29% and remained nearly constant at GDs from 29 to 36%.²⁴ However, the profiles showed only one peak, and thus a stacked lamellar model was proposed, with 480 nm diameter crystallites and a crystallite length outside the q -observation range ($d > 1.6 \mu\text{m}$) because the PTFE polymer, which has a very rigid conformation, cannot adopt a folding structure, as flexible polyolefins can. In contrast, ETFE contains flexible hydrocarbon main chains and thus crystallizes in a smaller lamellar size, as confirmed by FE-SEM images (vide infra).

Figures 8a and 8b show the surface FE-SEM images of the pristine ETFE and ETFE-PEM with an IEC of 2.4 mmol/g, respectively. The bright and dark areas in Figure 8a correspond to the areas with higher and lower electron densities, i.e., lamellar crystalline and amorphous phases with an approximate correlation distance of 18 nm, as explained in the SAXS profile discussion in the previous section. The ETFE-PEM showed an image similar to that of the pristine ETFE (Figure 8b). The membrane was stained with silver ions attached on the sulfonic acid groups, resulting in a higher contrast between the silver salt of the PSSA grafts in the lamellar amorphous domains and the lamellar crystalline domains, which were thus observed as

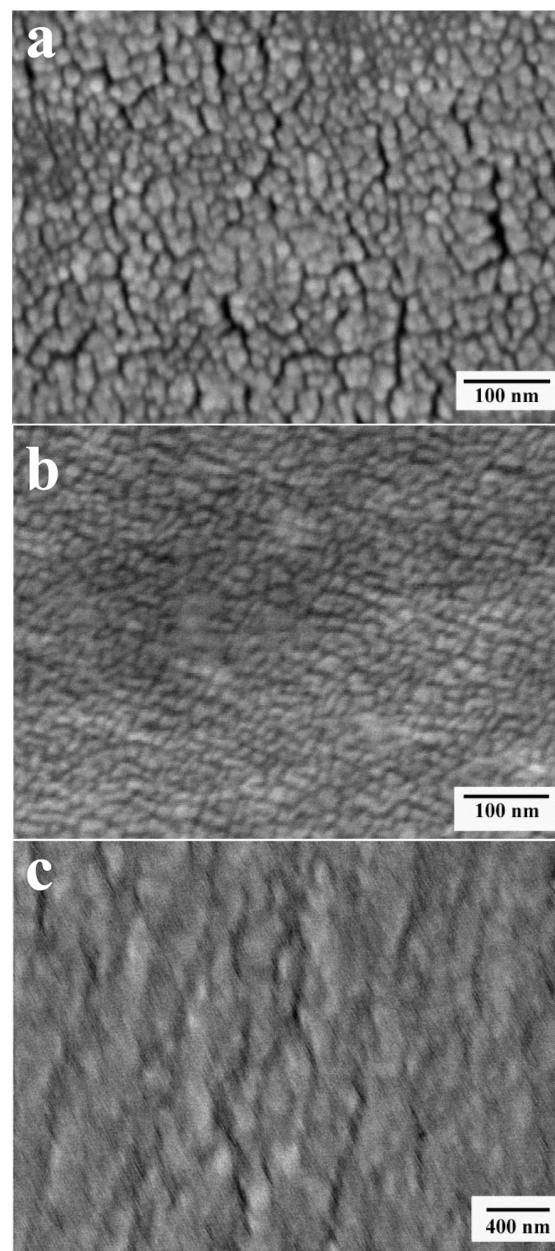


Figure 8. Surface FE-SEM images of the (a) original ETFE and (b) ETFE-PEM with an IEC of 2.4 mmol/g and a cross-section FE-SEM image of the ETFE-PEMs with IECs of 2.4 mmol/g.

bright and dark areas, respectively. It should be noted that the repeating structures originated from the PSSA grafts, as the influence of the lamellar structures in the pristine ETFE film was in good agreement with the SAXS profiles of these membranes.

In a magnified surface SEM image of the ETFE-PEM with an IEC of 2.4 mmol/g, the contrast seemed to be insufficient to discuss the oriented crystallite (lamellar grains) structure suggested by the USAXS profile. In contrast, as shown in the magnified cross-section SEM images in Figure 8c, for the membrane with an IEC of 2.4 mmol/g, the aligned bright stripes of 200–300 nm in width were clearly recognized and should correspond to ionic channels composed of grafted PSSA. The dark areas located between the bright ones are assigned to crystallite domains, judging from the electron density difference. Note that the graft polymer domains, with

similar repeating distances to the lamellar stacks and the oriented crystallites with a dimension of approximately 200–300 nm, are in good agreement with the size of the hierarchical structures determined by the SAXS measurements.

3.3. Structure–Property Relationships of Graft-Type ETFE-PEM

ETFE-PEM. It is well-recognized that PEMs in fuel cell applications require efficient proton conduction under low RH (<50% RH) and, at the same time, high inherent mechanical properties under humidified conditions (100% RH) and high temperatures (>80 °C). Accordingly, prior to the discussion on the relationship of the hierarchical structures of the graft-type ETFE-PEMs to the necessary properties for a PEM such as proton conductivity and mechanical strength on the basis of SAXS measurements and SEM observations, we plotted the (a) proton conductivities under 30% RH and (b) tensile strengths (TSs) under 100% RH at 80 °C as a function of the IEC of the ETFE-PEMs together with those of Nafion-212 as a reference (Figure 9); all the data were taken from a

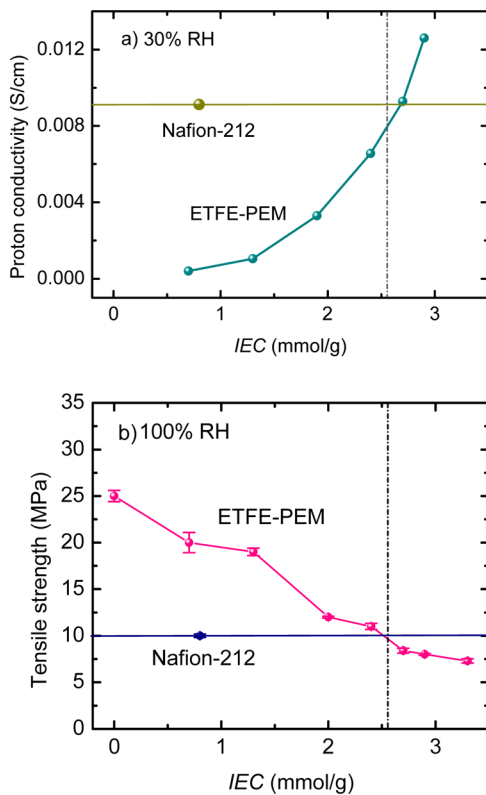


Figure 9. (a) Proton conductivity at 80 °C and 30% RH and (b) tensile strength at 80 °C and 100% RH of Nafion-212 and the ETFE-PEMs with IECs of 0–3.3 mmol/g.

previous report.¹⁷ The proton conductivities of the ETFE-PEMs with IECs of 1.3–2.9 mmol/g were 0.001–0.013 S/cm (Figure 9a). The conductance of the membranes increased with increasing IEC even at low RH (30% RH). The ETFE-PEMs with IECs higher than 2.7 mmol/g exhibited higher proton conductivity (0.0093 S/cm) than Nafion-212 (0.0090 S/cm). These conductivities are much higher than other aromatic hydrocarbon polymer-based PEMs (0.0001–0.001 S/cm) at similar IEC values.^{31,32}

As mentioned in section 3.2, the ETFE-PEMs with IECs greater than 2.7 mmol/g possess ion channels composed of PSSA grafts located outside of the crystallite network domains.

Thus, the high conductivity under low RH conditions (fewer water molecules) should result from the well-interconnected ion channels around the crystallites. It should be noted that this structural model for high conductivity with fewer water molecules is completely different from that for Nafion and aromatic hydrocarbon-type PEMs, in which phase-separated nanoscale ion channels are the origin of ion conducting paths with small amounts of water molecules under low RH conditions. In other words, this kind of hierarchical structure is expected to act as an effective route for higher proton transport through the ETFE-PEMs.

Although some of the electrolyte properties of PEMs can be elucidated from their structures in the dry state, it is also well-known that the electrolyte properties of hydrated PEMs differ significantly. Thus, the SAXS profiles of the hydrated ETFE-PEMs with IECs of 0–3.1 mmol/g (GDs of 0–117%) were measured and compared with those in the dry state (Supporting Information, Figure S3). The typical features in the SAXS profiles of the hydrated ETFE-PEMs were similar to those in the dry state over the entire range of IECs, except for the slightly lower q -positions of the distinct peaks and an increase in the scattering intensities $I(q)$ in the Lorentz-corrected SAXS profiles (Supporting Information, Figure S4). Accordingly, the ETFE-PEMs in the dry and hydrated states have quite similar characteristic lengths of the lamellar period and crystallite sizes (Supporting Information, Table S1). As shown in Figure 10, the expansion of the lamellar spacing of the

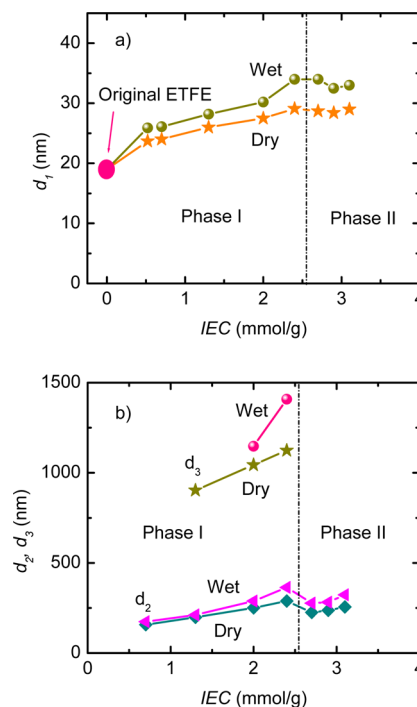


Figure 10. IEC dependences of the (a) lamellar periods (d_1) and (b) short (d_2) and long (d_3) correlation distances of the crystallites of the dry and wet ETFE-PEMs.

ETFE-PEMs due to water absorption increases from 23.5 to 31.1 nm with the increasing IEC (<2.4 mmol/g) and then remained constant in the IEC range of 2.4–3.1 mmol/g. Thus, the water absorption behavior in the lamellar stacks of the ETFE-PEMs did not change between phase I (IECs < 2.4 mmol/g) and phase II (IEC = 2.4–3.1 mmol/g). In contrast,

the correlation distances of the crystallites (d_2 and d_3) increased with increasing IEC in the range of 1.3–2.4 mmol/g in phase I, whereas after the phase transition (phase II), d_2 was constant in the IEC range of 2.4–3.1 mmol/g (Figure 10). However, the water uptake still increased from 74 to 145% in the IEC range of 2.4–3.1 mmol/g, as previously reported.¹⁷ The above results suggested that the further introduction of additional PSSA grafts with IECs > 2.4 mmol/g generated a new ion channel phase located outside of the crystallites. In other words, the model structure of phase II shown in Figure 7 possessed only PSSA graft domain, and most of the water was absorbed in this domain, resulting in no change in the correlation distances of the lamellar spacing (d_1) and crystallites (d_2).

In Figure 9b, the ETFE-PEMs with IECs of 0–2.4 mmol/g showed higher TSs (11–25 MPa) than Nafion-212 (10 MPa). In addition, the TS slightly decreased to 7.3 MPa at an IEC of 3.3 mmol/g in spite of the high water absorption.¹⁷ The excellent tensile strength of the ETFE-PEMs with high IECs in the hydrated state at high temperature must originate from the remaining lamellar stacks and crystallites (lamellar grains), as shown in Figure 10. Furthermore, as depicted in Figure 7, the ETFE-PEMs with GDs higher than 59% (IECs > 2.4 mmol/g) possess ion channels composed of PSSA grafts, located mainly outside of the crystallite network domains; thus, these additional ion channels, compared with the low IEC PEMs, effectively enhance the conductivity but do not degrade the lamellar stacks and crystallites. As a result, the crystallinity of the ETFE-PEMs did not decrease in the IEC range of 2.4–3.3 mmol/g. As previously reported,¹⁷ this is in good agreement with the behavior of the mechanical properties shown in Figure 9b. It should be noted that the lamellar stacks play an important role in maintaining a high inherent mechanical strength at higher swelling levels, especially for the PEMs with IECs (GDs) over 2.4 mmol/g (59%).

One disadvantages of the ETFE-PEMs with high IECs are low elongation at break under dry condition (<10%) even though that under a humid condition showed relatively high values (>250%), as previously reported.¹⁷ This is because, as mentioned in previous part, the well-connected and a large amount of PSSA graft polymer in ion channels are somewhat brittle under a dry condition.

To investigate where the absorbed water molecules are located in the hydrated ETFE-PEMs, the changes in the lamellar periods (d_1) and correlation distances of the crystallites (d_2 and d_3) as a function of the water absorption were evaluated quantitatively using the swelling ratio, i.e., the volume ratio of the hydrated and dried membranes, ϕ , according to the equation

$$\phi = \frac{\frac{m_{\text{PSSA}}}{\rho_{\text{PSSA}}} + \frac{m_{\text{ETFE}}}{\rho_{\text{ETFE}}} + \frac{m_{\text{water}}}{\rho_{\text{water}}}}{\frac{m_{\text{PSSA}}}{\rho_{\text{PSSA}}} + \frac{m_{\text{ETFE}}}{\rho_{\text{ETFE}}}} \quad (3)$$

where m_{PSSA} and ρ_{PSSA} are the weight and density of the PSSA grafts, m_{ETFE} and ρ_{ETFE} are the weight and density of the pristine ETFE, and m_{water} and ρ_{water} are the weight and density of the absorbed water.³⁰ The value of m_{PSSA} in eq 3 was determined from the GD using the equation

$$m_{\text{PSSA}} = \frac{m_{\text{SSA}} \times \text{DOG} \times m_0}{100 \times M_{\text{St}}} \quad (4)$$

where m_{SSA} and M_{St} are the molecular weights of a styrene sulfonic acid unit and a styrene unit, respectively. Here,

assuming isotropic swelling of the ETFE-PEMs, the one-dimensional swelling ratio, h , is calculated from ϕ using the following equation as a parameter to compare the real dimensional changes calculated from the SAXS profiles.³³

$$h = \sqrt[3]{\phi} \quad (5)$$

The ratios of each d -spacing of the hierarchical structures, i.e., the lamellar spacing (d_1) and the correlation distance of the crystallites (d_2) of the ETFE-PEMs in dry and wet conditions, were defined as expansion ratios $d_{1,\text{wet}}/d_{1,\text{dry}}$ and $d_{2,\text{wet}}/d_{2,\text{dry}}$, respectively (Supporting Information, Table S2). The expansion ratios are plotted with the one-dimensional swelling ratio, h , as a function of the IEC in Figure 11. As the IEC

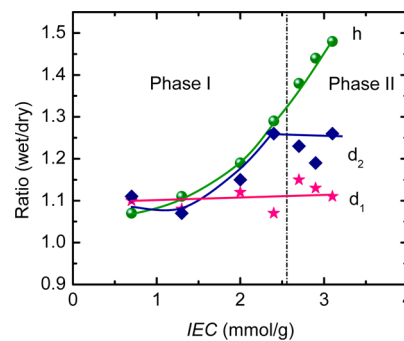


Figure 11. IEC dependences of the ratios between the wet and dry states of the lamellar period d_1 , correlation distance of the crystallites d_2 , and one-dimensional swelling ratio h .

increased from 0.7 to 3.1 mmol/g, h increased from 1.07 to 1.48. The expansion ratios of the lamellar period (d_1) were almost constant (approximately 1.1) over the entire IEC range, implying that the increase of d_1 is due to the presence of water molecules in the PSSA grafts around the lamellar crystals, which constitute less than 10% of the original PEM weight, even when the water uptake of the ETFE-PEMs increased from 0 to 145% as the IEC increased from 0 to 3.1 mmol/g.¹⁷ Thus, the very early stage of ion conductance of the PEMs with low IECs (<0.7 mmol/g) and low water uptakes (<13%) depends on the PSSA ion channels around the lamellar crystals. In contrast, the expansion ratios of d_2 in phase I increased from 1.11 to 1.26 with the increasing IEC from 1.3 to 2.4 mmol/g; this result agrees well with the increases of h . The ETFE-PEMs with IECs of 1.3–2.4 mmol/g showed conductivity that mainly depends on the amount of ion channels composed of PSSA grafts located in the oriented crystallites. Furthermore, the correlation distances of the crystallites (d_2) in phase II showed almost constant values in the ETFE-PEMs with IECs higher than 2.4 mmol/g (GDs > 59%). Noted that, for the ETFE-PEMs with higher IECs (>2.7 mmol/g), the increases of the membrane size by water absorption did not affect the size of the lamellar period (d_1) nor the correlation distance of the crystallites (d_2), strongly indicating that the PSSA grafts were mainly introduced at the outside of the crystallite network domains, which results in a high conductivity of the ETFE-PEMs with high IECs, as illustrated in Figure 7. It is noted that the proposed hierarchical structures of ETFE-PEMs are completely different from that of Nafion, for which the long parallel but randomly packed water channels surrounded by inverted-micelle cylinders of hydrophilic side branches³⁴ or ribbon-like aggregates surrounded by ionic groups packed with an orientation ordering in bundles^{35–37} are proposed for the origin of very high proton

conductivity at low water contents. For the ETFE-PEMs, the PSSA grafts containing water were found to localize in the lamellar amorphous domains in the crystallites for IECs lower than 2.4 mmol/g and were mainly generated at the outside of the crystallites for IECs higher than 2.7 mmol/g. This unique hierarchical structure of the ETFE-PEMs is favorable for the higher conductivity (>0.009 S/cm) at 30% RH and the compatible tensile strengths of approximately 8 MPa at 100% RH and 80 °C compared with Nafion.

4. CONCLUSION

The hierarchical structures of ETFE-PEMs with IECs less than 2.4 mmol/g were characterized as being composed of conducting PSSA graft domains around lamellar crystals with a period of 21.8–29.1 nm and oriented crystallites (lamellar grains) with short and long correlation distances of 218–320 and 903–1124 nm, respectively. The lamellar periods increased with increasing IEC (<2.4 mmol/g) and then remained constant in the IEC range of 2.4–3.1 mmol/g. These membranes with IECs > 2.7 mmol/g showed completely different scattering features, which were assigned to a new phase of crystallite network domains. These discontinuous changes of the crystallite size and scattering intensity in a low q -region strongly indicate a phase transition from oriented crystallite to crystallite network structures in the IEC range of 2.4–2.7 mmol/g. The SAXS observations over the whole q -region indicate that the ion channels consist of PSSA grafts localized around the lamellar crystals in the ETFE-PEMs with IECs < 2.4 mmol/g; they then expand to the outside of the crystallite network domains and have a higher interconnectivity for IECs > 2.7 mmol/g. From the SAXS/USAXS observations, it is revealed that for the ETFE-PEMs with high IECs (>2.7 mmol/g) a higher conductivity at 30% RH and compatible tensile strengths at 100% RH and 80 °C, compared with Nafion-212, originated from the well-interconnected ion channels around the crystallites and the remaining lamellar crystals and crystallites, respectively.

■ ASSOCIATED CONTENT

Supporting Information

SAXS profiles and data. This material is available free of charge via the Internet at <http://pubs.acs.org>.

■ AUTHOR INFORMATION

Corresponding Author

*E-mail: (Y.M.) maekawa.yasunari@jaea.go.jp.

Present Addresses

(T.D.T.) Department of Nuclear Engineering Physics, Faculty of Physics, University of Science Ho Chi Minh City, 227 Nguyen Van Cu, District 5, Ho Chi Minh, Viet Nam.

(Y.O.) Research Reactor Institute, Kyoto University, 2, Asashiro-Nishi, Kumatori-cho, Sennan-gun, Osaka 590-0494, Japan.

(M.O.) Graduate School of Engineering, Hokkaido University, Kita 13, Nishi 8, Kita-ku, Sapporo, Hokkaido 060-8628, Japan.

Notes

The authors declare no competing financial interest.

■ ACKNOWLEDGMENTS

This work was performed under the NIMS-RIKEN-JAEA Cooperative Research Program on Quantum Beam Science and Technology. The authors would like to thank Enago for the

English language review. The first author thanks Vietnam International Education Development (VIED) and Japan Atomic Energy Agency Fellow of Advanced Science (JFAS) for financial support of this work.

■ REFERENCES

- (1) Peckham, T. J.; Holdcroft, S. *Adv. Mater.* **2010**, *22*, 4667.
- (2) Borup, R.; Meyers, J.; Pivovar, B.; Kim, Y. S.; Garland, R. N.; Myers, D.; Wilson, M.; Garzon, F.; Wood, D.; Zelenay, P.; More, K.; Stroh, K.; Zawodzinski, T.; Boncella, J.; McGrath, J. E.; Inaba, M.; Miyatake, K.; Hori, M.; Ota, K.; Ogumi, Z.; Miyata, S.; Nishikata, A.; Siroma, Z.; Uchimoto, Y.; Yasuda, K.; Kimjima, K.; Iwashita, N. *Chem. Rev.* **2007**, *107*, 3904.
- (3) Li, Q.; He, R.; Jensen, J. O.; Bjerrum, N. *J. Chem. Mater.* **2003**, *15*, 4896.
- (4) Smitha, B.; Sridhar, S.; Khan, A. A. *J. Membr. Sci.* **2005**, *259*, 10.
- (5) Hasegawa, S.; Takahashi, S.; Iwase, H.; Koizumi, S.; Ohnuma, M.; Maekawa, Y. *Polymer* **2013**, *54*, 2895.
- (6) Tamada, M.; Maekawa, Y. Radiation Processing of Polymers and Its Applications. In *Charged Particles and Photon Interactions with Matter*; Hatano, Y., Katsumura, Y., Mozumder, A., Eds.; CRC Press: Boca Raton, FL, 2011; Chapter 27; pp 737–759.
- (7) Nasef, M. M.; Hegazy, E. A. *Prog. Polym. Sci.* **2004**, *29*, 499.
- (8) Chen, J.; Asano, M.; Yoshida, M.; Maekawa, Y. *J. Membr. Sci.* **2006**, *277*, 249.
- (9) Chen, J.; Asano, M.; Yoshida, M.; Maekawa, Y. *J. Appl. Polym. Sci.* **2006**, *101*, 2661.
- (10) Chen, J.; Septiani, U.; Asano, M.; Maekawa, Y.; Kubota, H.; Yoshida, M. *J. Appl. Polym. Sci.* **2006**, *103*, 1966.
- (11) Chen, J.; Asano, M.; Maekawa, Y.; Yoshida, M. *J. Membr. Sci.* **2007**, *296*, 77.
- (12) Kimura, Y.; Chen, J.; Asano, M.; Maekawa, Y.; Katai, R.; Yoshida, M. *Nucl. Instrum. Methods Phys. Res., Sect. B* **2007**, *263*, 463.
- (13) Gerald, A. N.; Zen, H. A.; Ribeiro, G.; Ferreira, H. P.; Souza, C. P.; Parra, D. F.; Santiago; Lugão, E. I. *Radiat. Phys. Chem.* **2010**, *79*, 246.
- (14) Gürsel, S. A.; Youcef, H. B.; Wokaun, A.; Scherer, G. G. *Nucl. Instrum. Methods Phys. Res., Sect. B* **2007**, *265*, 198.
- (15) Shen, M.; Roy, S.; Kuhlmann, J. M.; Scott, K.; Lovell, K.; Horsfall, J. A. *J. Membr. Sci.* **2005**, *251*, 121.
- (16) Lappan, U.; Geißler, U.; Gohs, U.; Uhlmann, S. *Radiat. Phys. Chem.* **2010**, *79*, 1067.
- (17) Tap, T. D.; Sawada, S.; Hasegawa, S.; Katsumura, Y.; Maekawa, Y. *J. Membr. Sci.* **2013**, *447*, 19.
- (18) Jokela, K.; Serima, R.; Torkkeli, M.; Sundholm, F.; Kallio, T.; Sundholm, G. *J. Polym. Sci., Polym. Phys. Ed.* **2002**, *40*, 1539.
- (19) Balog, S.; Gasser, U.; Mortensen, K.; Gubler, L.; Scherer, G. G.; Youcef, H. B. *Macromol. Chem. Phys.* **2010**, *211*, 635.
- (20) Balog, S.; Gasser, U.; Mortensen, K.; Youcef, H. B.; Gubler, L.; Scherer, G. G. *J. Membr. Sci.* **2011**, *383*, 50.
- (21) Balog, S.; Gasser, U.; Mortensen, K.; Youcef, H. B.; Gubler, L.; Scherer, G. G. *Polymer* **2012**, *53*, 175.
- (22) Sawada, S.; Yamaguchi, D.; Putra, A.; Koizumi, S.; Maekawa, Y. *Polym. J.* **2012**, *45*, 797.
- (23) Song, J. M.; Ko, B. S.; Sohn, J. Y.; Nho, Y. C.; Shin, J. *Radiat. Phys. Chem.*, in press.
- (24) Iwase, H.; Sawada, S.; Yamaki, T.; Koizumi, S.; Ohnuma, M.; Maekawa, Y. *Macromolecules* **2012**, *45*, 9121.
- (25) Zhang, F.; Ilavsky, J.; Long, G. G.; Quintana, J. P. G.; Allen, A. J.; Jemian, P. R. *Metall. Mater. Trans. A* **2010**, *41A*, 1151.
- (26) Matyi, R. J.; Crist, B. J. R. *J. Polym. Sci., Polym. Phys. Ed.* **1978**, *16*, 1329.
- (27) Cser, F. *J. Appl. Polym. Sci.* **2001**, *80*, 2300.
- (28) Tigelaar, D. M.; Parker, A. E.; He, R.; Scheiman, D. A.; Petek, T.; Savinell, R.; Yoonessi, M. *J. Membr. Sci.* **2011**, *369*, 455.
- (29) Okabe, Y.; Murakami, H.; Osaka, N.; Saito, H.; Inoue, T. *Polymer* **2010**, *51*, 1494.

- (30) Cheung, Y. W.; Stein, R. S.; Lin, J. S.; Wignall, G. D. *Macromolecules* **1994**, *27*, 2520.
- (31) Miyatake, K.; Bae, B.; Watanabe, M. *Polym. Chem.* **2011**, *2*, 1919.
- (32) Suda, T.; Yamazaki, K.; Kawakami, H. *J. Power Sources*. **2010**, *195*, 4641.
- (33) Youcef, H. B.; Gürsel, S. A.; Wokaun, A.; Scherer, G. G. *J. Membr. Sci.* **2008**, *311*, 208.
- (34) Rohr, K. S.; Chen, Q. *Nat. Mater.* **2008**, *7*, 75.
- (35) Rubatat, L.; Rollet, A. L.; Gebel, G.; Diat, O. *Macromolecules* **2002**, *35*, 4050.
- (36) Gebel, G.; Diat, O. *Fuel Cells* **2005**, *5*, 261.
- (37) Rubatat, L.; Li, C.; Dietsch, H.; Nykänen, A.; Ruokolainen, J.; Mezzenga, R. *Macromolecules* **2008**, *41*, 8130.